Novel infrared-terahertz fusion 3D non-invasive imaging of plant fibre-reinforced polymer composites

Jue Hu, Hai Zhang, Stefano Sfarra, Carlo Santulli, Guiyun Tian, Xavier Maldague

PII: S0266-3538(22)00268-8

DOI: https://doi.org/10.1016/j.compscitech.2022.109526

Reference: CSTE 109526

To appear in: *Composites Science and Technology*

Received Date: 22 October 2021

Revised Date: 14 March 2022

Accepted Date: 11 May 2022

Please cite this article as: Hu J, Zhang H, Sfarra S, Santulli C, Tian G, Maldague X, Novel infrared-terahertz fusion 3D non-invasive imaging of plant fibre-reinforced polymer composites, *Composites Science and Technology* (2022), doi: https://doi.org/10.1016/j.compscitech.2022.109526.

Jue Hu: Methodology, Software, Formal analysis, Investigation, Writing - Original draft preparation. Hai Zhang: Conceptualization, Validation, Investigation, Writing - Reviewing and Editing, Supervision, Project administration. Stefano Sfarra: Investigation, Resources, Visualization, Writing - Review & Editing. Carlo Santulli: Resources, Writing-Reviewing and Editing. Guiyun Tian: Writing-Reviewing and Editing, Supervision. Xavier Maldague: Writing-Reviewing and Editing, Supervision, Project administration, Funding acquisition.

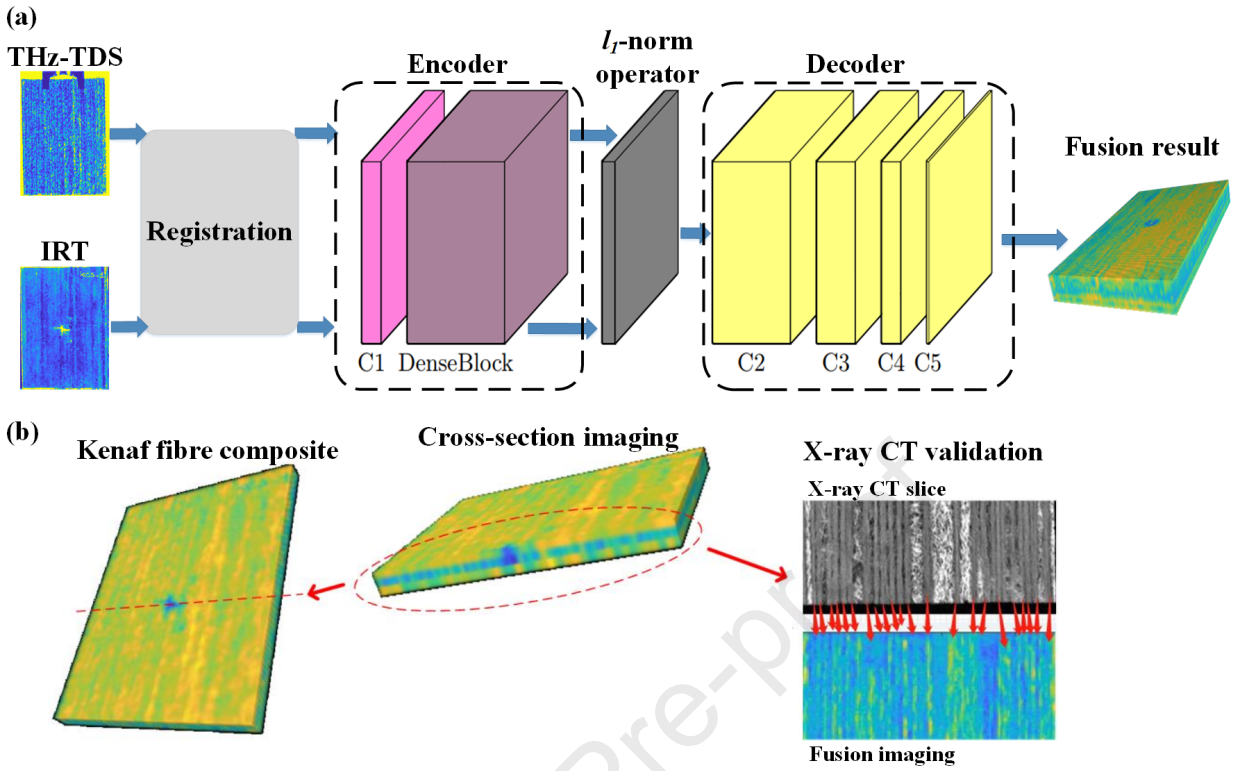

Novel infrared-terahertz fusion 3D non-invasive imaging of plant fibre-reinforced polymer composites

Jue Hu [a,b], Hai Zhang [c,b,*], Stefano Sfarra [d], Carlo Santulli [e], Guiyun Tian [a,f], Xavier Maldague [b]

[a] *School of Automation Engineering, University of Electronic Science and Technology of China, Chengdu 611731, China*

[b] *Department of Electrical and Computer Engineering, Computer Vision and Systems Laboratory, Laval University, Quebec, G1V 0A6, Canada*

[c] *Centre for Composite Materials and Structures, Harbin Institute of Technology, Harbin 150001, China*

[d] *Department of Industrial and Information Engineering and Economics (DIIIE), University of L'Aquila, Piazzale E. Pontieri 1, Monteluco di Roio, 67100 L'Aquila, AQ, Italy*

[e] *School of Architecture and Design, University of Camerino, 63100 Ascoli Piceno, Italy*

[f] *School of Engineering, Newcastle University, Newcastle upon Tyne NE1 7RU, UK*

Abstract

The reinforcement of polymer composites using plant fibres has received vast and growing attention for investigation owing to their capability to serve as semi-structural materials, especially as a substitute for fiberglass. However, in this type of research, the structural complexity, due to geometrical mismatches and inherent variability to the properties of vegetable fibres and plant fibre composites would benefit from more effective non-invasive inspection techniques. In this work, a novel infrared-terahertz fused approach was proposed, and a new unsupervised deep residual fusion algorithm was developed in order to combine the outputs from two different physical mechanisms. Specifically, infrared imaging provided the details of the defects and the morphological information from the surface and subsurface, while terahertz imaging recorded the distribution of the fibres and the resin. Finally, the fused infrared-terahertz slices were reconstructed into a form of 3D exhibition for inspection and evaluation of two plant

* Corresponding author: hai.zhang.1@ulaval.ca

fibre-reinforced polymer composites.

Keywords: Jute fibre; kenaf fibre; non-destructive inspection; infrared; terahertz.

1. Introduction

In recent years, plant fibre-reinforced polymer (PFRP) composites have received vast and growing attention for investigation owing to the potential of serving as semi-structural materials. PFRP has many advantages including the fact that it is environmentally friendly, lightweight and low cost, *etc*. Several investigations of PFRP such as coir, hemp, jute and bamboo have already been presented to reveal the mechanical properties and the possible role and use of non-destructive inspection (NDI) on manufactured composites [1]. However, internal manufacturing inspection is still a problem. Therefore, NDI needs to be conducted in order to broaden the field for the application of PFRP.

Advances in NDT inspection on composite structures have been reviewed by several researchers [2–5]. In composite structure inspection, X-ray is widely adapted for computed tomography (CT) [6]. This technique has the ability to provide promising results with the 3D structure of the specimen. However, the ionizing radiation and high price of the equipment still restrict the application [7]. Ultrasonic scanning is another common approach for composite inspection when considering safety and low cost while the dependence on the coupling medium such as water limits the application of this inspection technique to waterproof materials [8]. In the last few decades, infrared thermography (IRT) has been developed as a non-invasive and non-contact inspection method [9,10]. Several techniques such as optical excitation thermography (OET)

[11,12], laser excitation thermography [13], ultrasonic excitation thermography [14] and eddy current excitation thermography (ECT) [15] have been applied in the evaluation of composites. Nevertheless, IRT is not ideal for transparent and semi-transparent materials like glass fibre reinforced composites [8]. In addition, limited penetration capability restricts the inspection depth of IRT [16], which actually provides the surface and the sub-surface information for evaluation. Terahertz time-domain spectroscopy (THz-TDS) has attracted more attention for composite evaluation in recent years, since it is safer than X-rays and offers a stronger capability of penetration than IRT [17–19].

As is widely recognized, neither a single sensor nor an individual measurement system can fully characterize object for NDI [20]. Recently, Wang et al. proposed a fusion method involving THz and X-ray data for non-destructive evaluation of glass fibre reinforced polymer (GFRP) [21]. This method was based on a hybrid model, which combines the merits of saliency region analysis and multi-scale transforms to obtain high contrast defect information of GFRP composite. The quantitative evaluation proved that the design of the average gradient strategy for high frequency sub-band and contrast strategy for low frequency sub-band effectively improved the performance.

In this work, a novel IRT and THz-TDS fusion NDI technique was proposed for plant fibre composite inspection. The data from IRT provided the details of the defects and the morphological information from both the surface and subsurface. The data from THz-TDS recorded the distribution of the fibres and the resin at deeper depths. The information extracted from the two techniques was pre-processed and then fused with

a newly developed unsupervised deep neural network. The output of the network combines the morphological characteristics of the defects with the distribution of the fibres. The fusion results provided the inspection along with the thickness of the materials, which can be used for tomography later. The experiments were carried out on two plant fibre composite samples to reveal the effectiveness of the proposed technique. The fusion results showed that the new technique significantly improved the detection capability.

The main contributions of this work can be concluded as follows. First, we proposed an infrared-terahertz fusion NDI technique, which is superior for the inspection of complicated composite structures. Second, an unsupervised deep residual fusion algorithm was specifically developed for the new NDI technique. Finally, the fusion results were reconstructed to provide a 3D exhibition of the through-depth inspection, which is helpful to better understand the characteristics of the composite structures.

2. Materials

As illustrated in Fig. 1 and Table 1, the specimens involved in this study include jute and kenaf fibre laminates [22]. The sample illustrated in Fig. 1(a) was manufactured with jute/glass hybrid fibre. The composite was laminated by the sequence of surface veil, chopped strand matrix and jute fibre. Another sample illustrated in Fig. 1(b) was prepared with kenaf/glass hybrid fibre. A sandwich structure is adapted to construct the laminate. The core was fabricated with continuous kenaf/glass hybrid fibre yarns whereas the two skins were made of chopped strand

matrix with a surface veil. Unsaturated polyester resin Crystic P9901 produced by Scott Bader (UK) was used for the fabrication of all laminates. A protection surface veil in jute/glass hybrid composite was composed of glass fibre mesh with a thickness of 0.2 mm. The glass fibre mesh was supplied by Sika Kimia Sdn. Bhd. Lot 689, Nilai Industrial Estate, 71800 Nilai Negeri Sembilan D.K., Malaysia. The surface veil in kenaf/glass hybrid composite was made of polyester fibres using a non-woven process and was then finished with resin. The final thickness obtained for this layer was 0.1 mm. Chopped strand matrices were supplied by Hengshui Yixing Fibreglass Co. Limited (China), jute fibres were produced by Alam Fibre Impex Ltd., while kenaf fibres were prepared by the Malaysian Tobacco Board in twisted roving form. The thread diameters of jute and kenaf were approximately 1 mm and 2 mm, respectively.

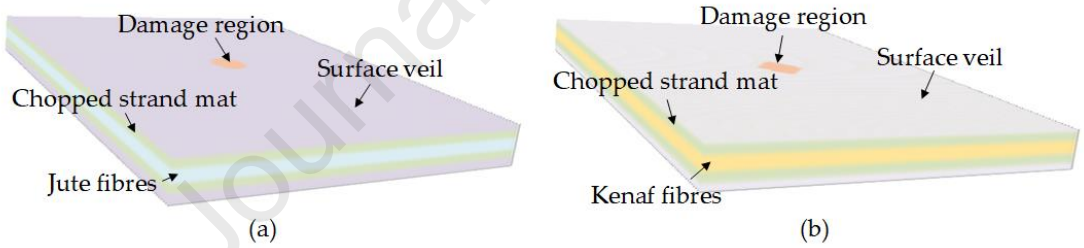

Figure 1: Structure of specimens used in this study: (a) Jute composite; (b) Kenaf composite.

Table 1. Laminates configuration.

Configuration code	Stacking sequence	Thickness (mm)	Fibre content (wt.%)
JC	S/C/J/J/C/S	2.80±0.02	40 jute + 25 glass
KCS	S/C/K/C/S	2.80±0.02	40 kenaf + 25 glass

J = Jute fibres, C = chopped strand mat, K = kenaf fibres, S = surface veil.

As illustrated in Fig. 2, both of these laminates were impacted with a falling weight impact energy equal to 12 Joules, hence creating visible indentation damage: the different appearance of the laminates was caused by the discrepant characteristics on energy absorption.

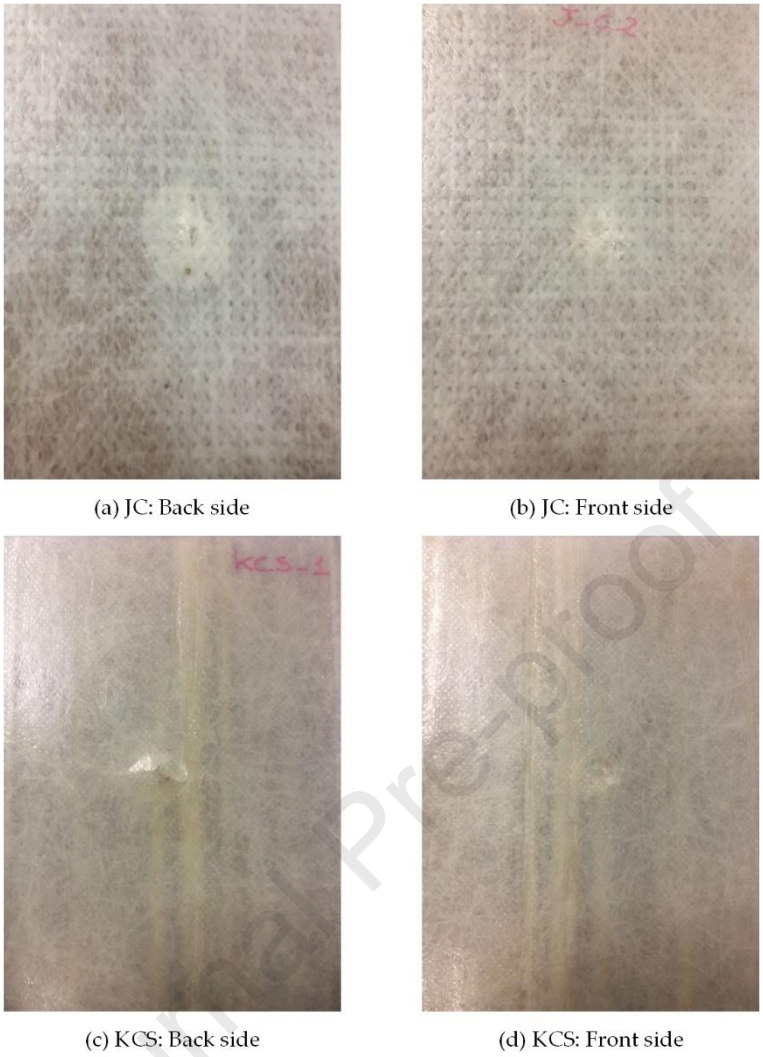

Figure 2: (a)-(b) Jute fibre composite; (c)-(d) Kenaf fibre composite.

3. Methodology

In this study, a multi-modality spatial-spectral data fusion technique was developed. The complete schematic diagram of the newly developed technique is shown in Fig. 3. Raw data collected from the THz-TDS system was analysed in both the time-domain and the frequency-domain in order to obtain the images based on different time domain representations and spectral characteristics of the materials. The obtained thermal sequence from the IRT system was also analysed in order to image the different depths. Then, the analytical results from THz-TDS and IRT were pre-processed to confirm that the images from different techniques were in strict

geometrical alignment and intensity matching. An unsupervised deep residual fusion network was developed to fuse the images from different techniques and then the fusion results were reconstructed in the form of 3D to show the through-depth exhibition of the materials. The details of the physical mechanism and the processing procedure will be discussed in this section.

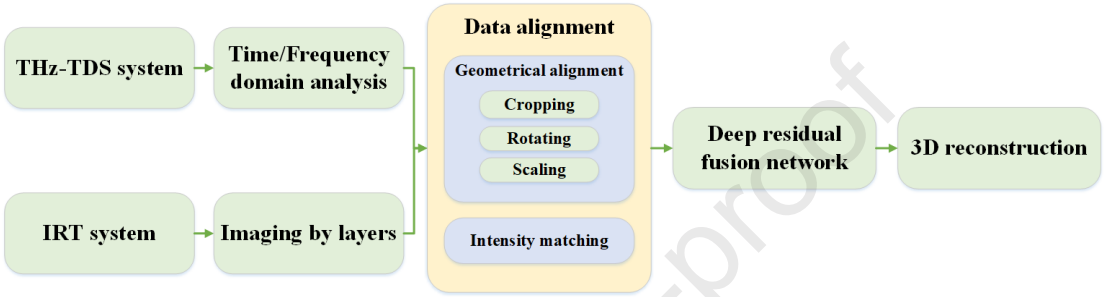

Figure 3: Schematic diagram of the proposed multi-modality spatial-spectral data fusion technique.

3.1 Terahertz time-domain spectroscopy (THz-TDS)

The THz-TDS imaging system is shown in Fig. 4. The ultra-fast laser pulse is split into a pump beam and reference beam. The pump beam is time-shifted using an optical time-delay line and then adapted to excite a THz pulse using a THz emitter. The THz wave crosses through the sample and detects with a coupled detector. The reference beam is implemented here on the detector as the sampling signal. The THz signal after sampling is transferred to a lock-in amplifier. Amplification of the weak signal is carried out for data acquisition.

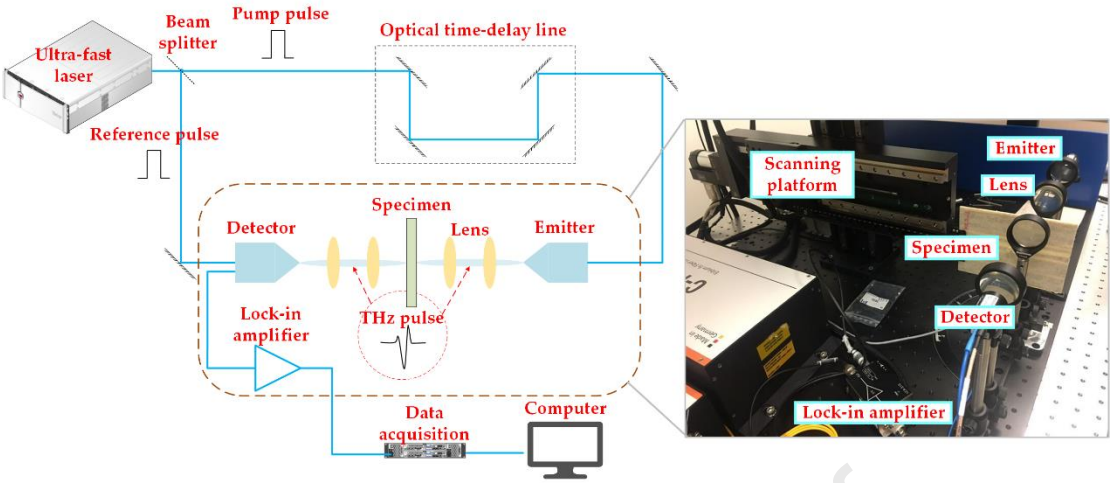

Figure 4: Schematic and experimental setup of the THz-TDS system used herein.

The THz-TDS system was manufactured by Menlo Systems GmbH, Munich, Germany. The system has a 1.2 GHz frequency resolution and the repetition rate is 100 MHz. The experiments were performed in both transmission and reflection mode. The scanning step is set as 0.5 mm.

3.2 Infrared thermography (IRT)

Fig. 5 shows the experimental configuration of the PT imaging system. Two flash units (Balcar FX60, 6.4 kJ, 2 ms duration) were used to generate optical flashes in this configuration. A mid-wave IR camera (FLIR Phoenix) with a frame rate of ~55 Hz and the NETD of 25 mK was adapted to record the temperature profile. The cooling time was set at 10 s for flashes. The camera spatial resolution was 640 × 512 pixels (25 μm × 25 μm of detector size) and a 50 mm lens was employed to provide a field of view (FOV) of 18.2° (horizontal) × 14.6° (vertical).

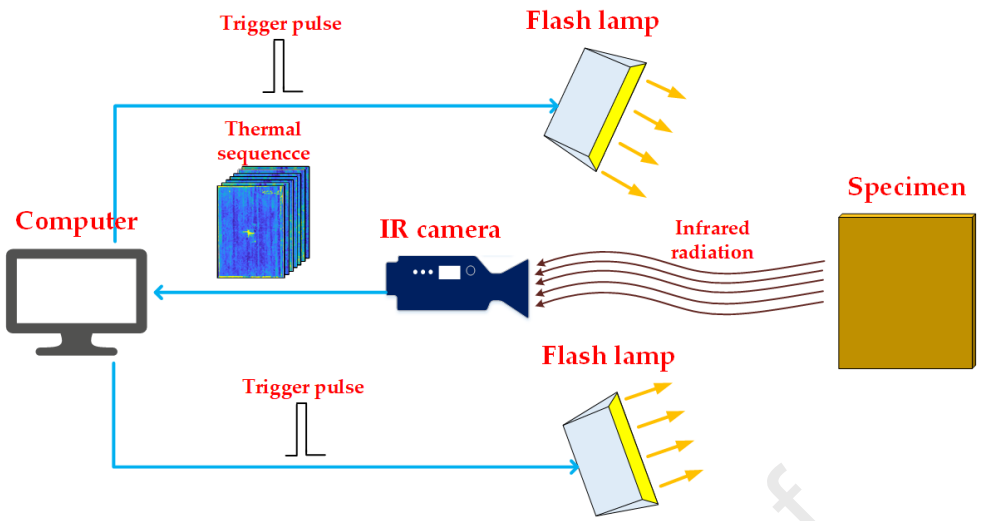

Figure 5: Configuration of the IRT experimental system used herein.

3.3 Unsupervised deep residual fusion algorithm

As illustrated in Fig. 6, the analytical results from THz-TDS and IRT were pre-processed to confirm that the images for fusion were in strict geometrical alignment and intensity matching. In this study, the geometrical alignment was conducted by matching the control points (CPs) from the contours of the sample. During the alignment process, we fixed the terahertz images, and then registered the infrared images to the terahertz images. The details of the alignment process can be described as follows. First, we selected several CPs manually from the contours of the samples on the images provided by THz and IRT systems. Then, we calculated the transform from the selected CPs on IRT to the selected CPs on fixed THz imaging, by using the operators such as stretching, rotating and scaling. Finally, we adapted the transform calculated from the selected CPs to the whole IRT images. The color bar was then matched to obtain the intensity alignment image for fusion. The above pre-processing procedures were conducted using Matlab software. In the fusion stage, an unsupervised encoder-decoder network architecture was introduced. The encoder including a

convolutional layer and a dense-connected block extracted high-dimensional features on images from different modalities. Then, these high-dimensional features were fused with an l_1-norm based fusion rule and reconstructed by the decoder, which is composed of convolutional layers.

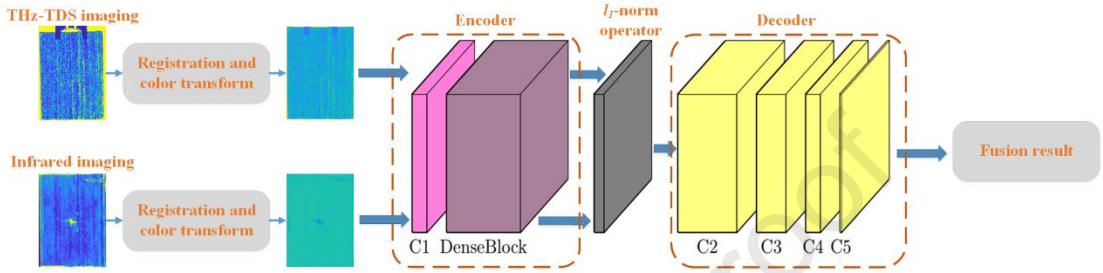

Figure 6: Diagram of the unsupervised deep residual fusion algorithm

The encoder illustrated in Fig. 7 combines dense connections with residual modules to extract high-dimensional features from input images. Residual learning can optimize several convolutional layers as identity mapping which eases the training of the deep neural network and benefits from increasing depth [23]. Dense connections between residual blocks ensure that the input of each residual block is the concatenation of all of the former modules [24]. This effectively protects the information in the middle layer from vanishing and sufficiently extracts salient features.

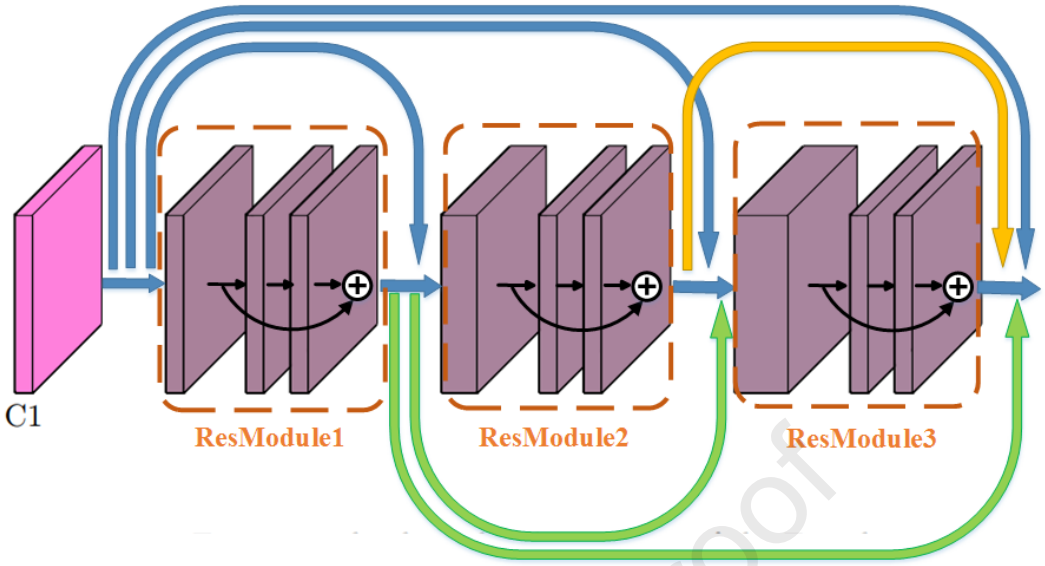

Figure 7: Structure of the encoder

The fusion layer is constructed with an operator based on l_1-norm. First, the l_1-norm map of each point (x, y) is calculated on the features extracted by the encoder. The activity level map $M_i(x, y)$ for each source is calculated using a blocked average operator rolling on the l_1-norm map:

$$M_i(x,y) = \frac{\sum_{a=x-1}^{x+1}\sum_{b=y-1}^{y+1}\|\Phi_i^{1:N}(a,b)\|_1}{9} \quad (1)$$

where Φ_i^n $(i = 1, \cdots, k)$ refers to the feature map calculated by the encoder of the i-th input source, $k \geq 2$ indicates the total number of the input modalities, $n = 1,2, \cdots, N$ $(N = 64)$ indicates the index of the specific feature belonging to the feature map, and N denotes the total number of the features generated by the encoder per input.

Then, the weighted mask $W_i(x, y)$ for each source is calculated by:

$$W_i(x,y) = \frac{M_i(x,y)}{\sum_{j=1}^{k} M_j(x,y)} \quad (2)$$

while, the fused feature map $\Phi_f^n(x, y)$ is obtained as follows:

$$\Phi_f^n(x,y) = \sum_{i=1}^{k} W_i(x,y)\,\Phi_i^n(x,y) \quad (3)$$

The fused feature map is then processed by the decoder to reconstruct the fusion

image, which effectively contains the information provided by different sensors. The decoder in a concise and efficient architecture includes four convolutional layers with a decreasing number of output features as 64, 32, 16 and 1.

In the training process, the fusion layer based on the l_1-norm operator would be removed. The encoder and decoder are directly stacked to train the weights of the convolutional layers. This process is aimed at ensuring that the Encoder-Decoder network can extract salient features of the input images and use these features to reconstruct the images. To achieve this, the total loss function formulated in Eq.4 needs to be minimized, which is a weighted combination of the structural similarity loss L_{SSIM} and pixel loss L_P.

$$L_{total} = \lambda L_{SSIM} + L_P \tag{4}$$

where, λ refers to the magnitude difference between the structural similarity loss and the pixel loss. $\lambda = 1$ is adopted in this work.

The pixel loss is calculated using l_2-norm to measure the difference between the input and output matrix as follows:

$$L_P = \|O - I\|_2 \tag{5}$$

where I indicates the raw image and O refers to the image reconstructed by the Encoder-Decoder network.

The structural similarity loss is calculated as in [25]:

$$L_{SSIM} = 1 - SSIM(O - I) \tag{6}$$

where, $SSIM(O - I)$ refers to the structural similarity operator which is a perceptual measurement of the similarity of the fused image and input image. It aims at enabling the network to extract the representation and to reconstruct the image considering both

the local structure and contrast. The network in the Encoder-Decoder structure is trained on the dataset containing 142776 grayscale images of MS-COCO [26].

4. Experimental results and discussion

Fig. 8 illustrates the THz-TDS analysis process of the raw data collected from the experimental system working in transmission mode. The analysis includes both time-domain imaging and frequency-domain analysis. In the jute fibre composite illustrated in Fig.8 (a), the time-domain curve of spatial location on the chopped glass fibre shows a larger time delay. In order to utilize this, the arrival time (38.73 ps) of the peak on the time-domain curve of chopped glass fibre is chosen for imaging on the chopped glass fibre layer. The frequency-domain curve reflects the different characteristics in the absorption of variant materials. The woven roving appears to have a higher absorption at 0.44 THz due to the high absorption coefficient of woven roving material at this point in the spectrum. Therefore, the spectral amplitude image at this point is adapted for imaging on the woven roving layer. In the kenaf fibre composite illustrated in Fig.8 (b), the time-domain curve of the spatial location on kenaf yarn reveals a larger time delay than that of other materials. With this in mind, the corresponding arrival time (78.43 ps) of the peak on the time-domain curve of kenaf yarn is selected for imaging on the kenaf yarn layer. The chopped strand matrix shows obvious absorption at 0.48 THz in the spectrum. This motivates us to use the spectral amplitude image at this point for imaging on the chopped strand matrix layer.

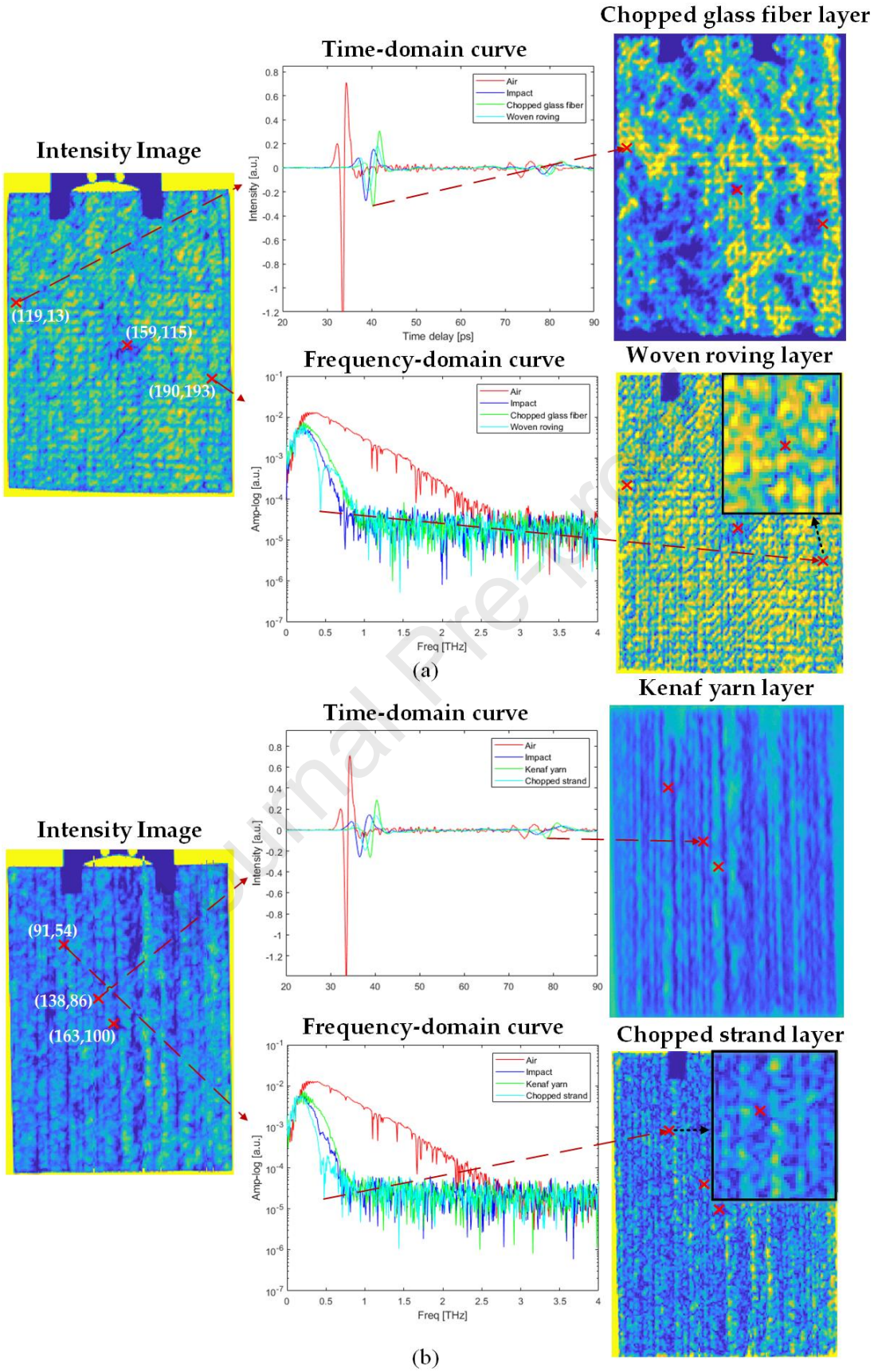

Figure 8: THz-TDS analysis: (a) Jute composite sample; (b) Kenaf composite sample.

In order to obtain further complementary information on different depths, we also

carried out experiments in the THz reflection mode. As illustrated in Fig. 9, THz waves produce reflection on the boundary of different media. The first reflection wave generated at the junction of air and the surface veil layer carries the information of the glass fibre mesh on this layer. The second reflection wave generated on the boundary of the surface veil and chopped strand mat layers contains the information of the fibre distribution on the chopped strand mat layer. The mask box in Fig.9 shows that time-gated Fourier transform [27] was carried out for amplitude imaging on the reflected waves. The curves used here are collected from the THz experiment on the reflection mode of jute fibre composite on the backside view. The same processes are repeated on the front view data of the jute fibre composite, including both back and front view data of the kenaf fibre composite.

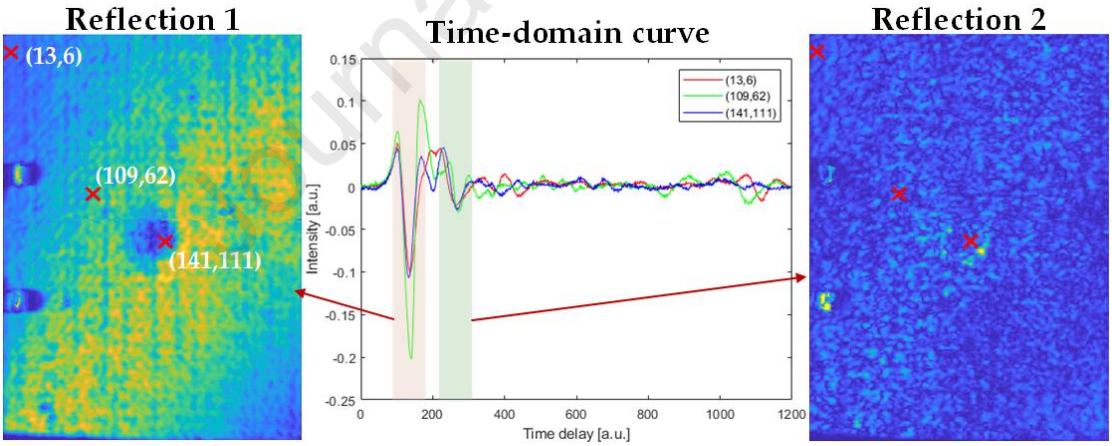

Figure 9: THz-TDS analysis in the reflection mode using time-gated Fourier transform on the backside view of the jute composite sample.

The analysis of the raw data collected from IRT is introduced in Fig. 10. With the thermal diffusion process, IRT can present information at different depths. In this work, optical excitation thermography is conducted on both sides of the specimens. The view of the thermal sequence collected from both sides is flipped on the back-side view.

Readers should note that the second frame was selected as the surface information, while the hundredth frame was chosen as the subsurface information. In the jute composite, surface information includes the impact-induced damage and the air holes existing in cured resin in the form of hot spots. Sub-surface information mainly contains impact-induced damage and slight traces of woven roving. In the kenaf composite, surface information includes impact-induced damage, air holes and the mark created by ink, while subsurface information mainly contains the impact area.

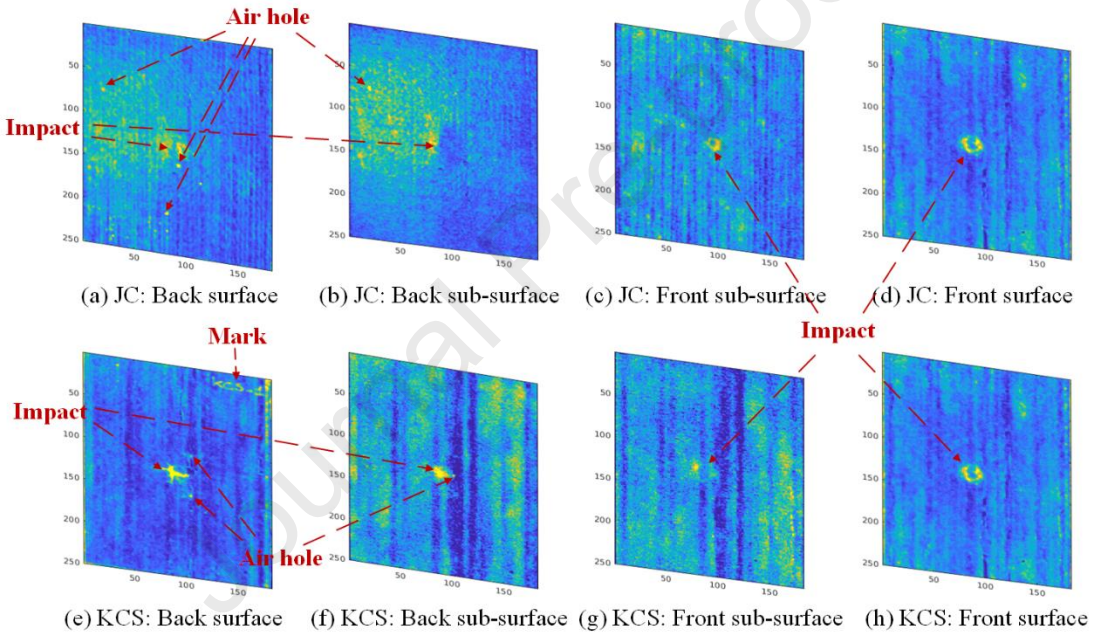

Figure 10: IRT results: (a)-(d) Jute composite sample; (e)-(h) Kenaf composite sample.

In Fig. 11, the 3D fusion imaging results on the jute fibre composite are shown. The left part shows the 3D reconstruction result with the impact region and air holes on the surface. The surface veil made of glass fibre mesh can also be seen on the surface of the reconstruction result. On the right part, the 3D reconstruction model is cut at the chopped strand mat layer, and then compared with the X-ray CT inspection at a depth of 0.4 mm from the backside of the sample. It is worth noting that, other than the impact

region, the chopped glass fibre distribution on the CT inspection result can also be mapped by the chopped strand mat layer on the 3D fusion imaging.

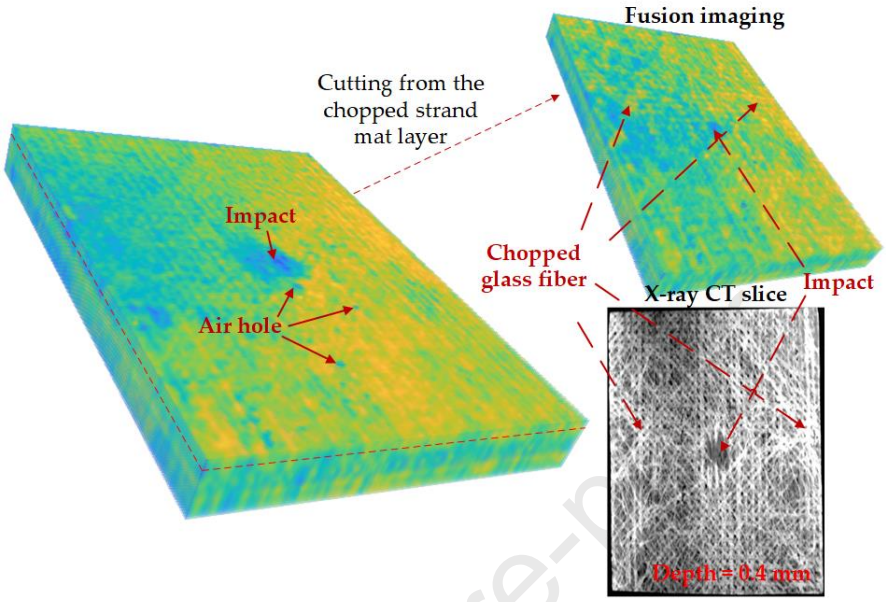

Figure 11: 3D fusion imaging of the jute fibre composite and the comparison with the X-ray CT slice.

The 3D reconstruction results of the kenaf fibre composite are shown in Fig. 12. In the middle row of the figure, we list the images observed from different views of the 3D reconstruction model. A more intuitive representation can be found in the video in the supplementary materials. In the top row of the figure, the 3D reconstruction result is cut on the chopped strand mat layer and the kenaf yarn layer, respectively. Fig. 12(a) is cut on the chopped strand mat layer and compared with the CT slice at a depth of 0.8 mm from the back panel. The low-velocity impact-induced damage and banded dent observed in IRT imaging are merged with the glass fibre content distribution viewed in THz imaging. All of these patterns are presented on the fusion imaging result and can be mapped by the referred X-ray CT slice. Fig. 12(b) is a cut on the kenaf yarn layer, which refers to the CT slice obtained at a depth of 1.6 mm from the back panel. It is worth mentioning that, as an internal layer, the kenaf yarns in this layer are observed

clearly with the impact-induced damage in the 3D fusion result. In the bottom row of the figure, we further present the cross-section imaging and horizontal-section imaging of the 3D reconstruction result. Fig. 12(c) shows the cross-section imaging cut at the position of 71.5 mm and 88.5 mm from the upper edge of the sample. Interestingly, the position of 71.5 mm from the upper edge is exactly the location of the impact-induced damage. Therefore, the morphology of the impact can be observed on this cross-section imaging. Fig. 12(d) presents the horizontal-section of the kenaf fibre yarns layer. As an internal layer in such a 3D structure with complicated fibre content, the kenaf yarn layer with rich plant fibre information is chosen for the detailed comparison with the CT slice. The kenaf yarns present on the cropped horizontal-section of the 3D fusion imaging and the cropped CT slice are matched with a red arrow. A total of 26 kenaf yarns can be mapped into the X-ray CT inspection result one-by-one. This illustrates that the proposed 3D fusion imaging technique generates high quality images on the internal structures. The fusion of the information from complementary depths of different imaging systems paves the way for conducting high contrast and high resolution imaging on the hybrid laminates.

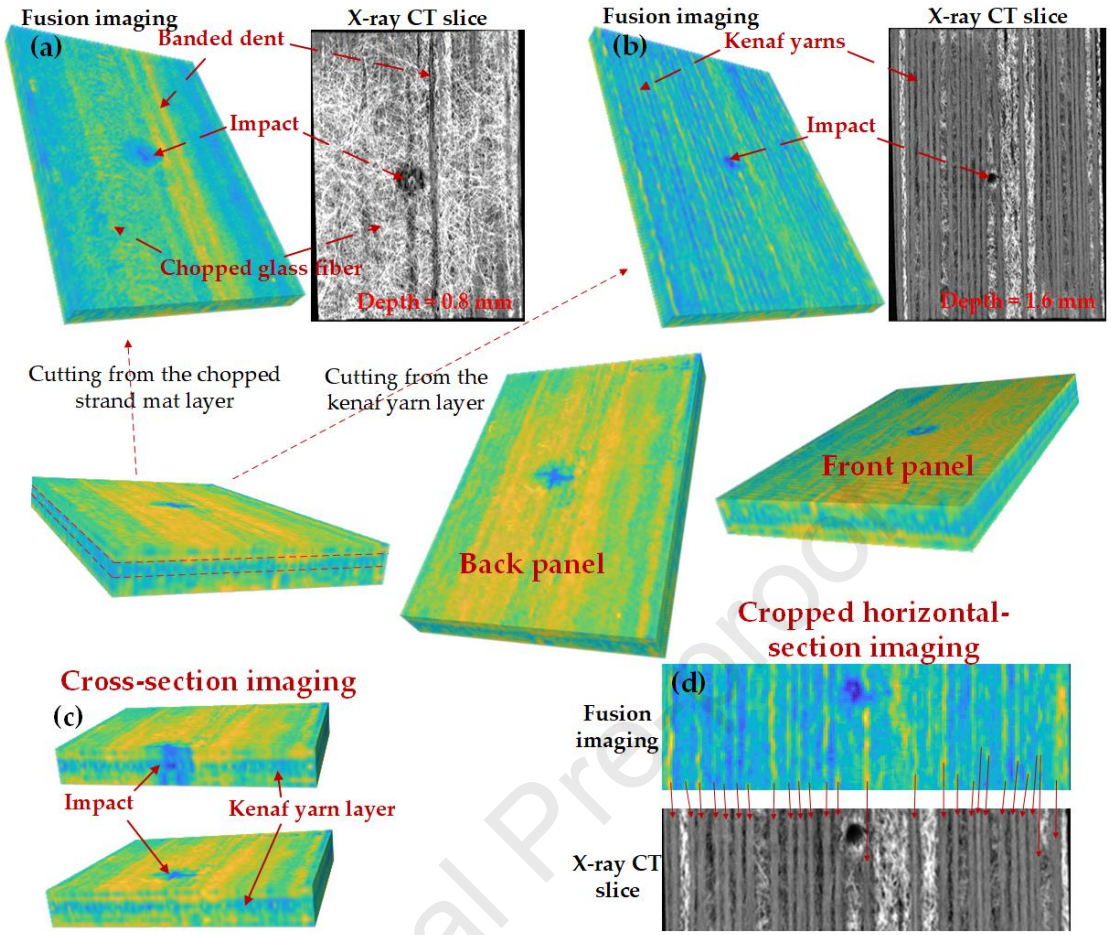

Figure 12: 3D fusion imaging results on the kenaf fibre composite. Images in the middle row refer to the 3D model from different observation views. The top row illustrates the comparison of the 3D reconstruction results cut from different layers and the X-ray CT imaging. The bottom row shows the cross-section and horizontal section of the kenaf fibre composite.

In addition to the qualitative comparison, a quantitative evaluation with the signal-to-noise ratio (SNR) [8] was also carried out to characterize the fusion performance. On each sample, we calculated SNR at various depths and then obtained the averaged SNR. The results are shown in Table 2.

Table 2. Comparison based on averaged SNR of different samples.

Evaluating Index	Jute composite		Kenaf composite	
	Fusion	X-ray CT	Fusion	X-ray CT
Averaged SNR	44.56	46.19	44.28	45.25

It can be observed that, in both the qualitative and quantitative comparison, the proposed technique as a non-invasive method led to a performance which was

comparable to the performance obtained with the X-ray CT. In general, the proposed fusion imaging method can be a potential substitute for ionizing X-ray analysis in nondestructive evaluation of plant fibre reinforced composites.

5. Conclusions

In this work, a multi-modality unsupervised spatial-spectral data fusion technique was developed for plant fibre composite inspection using data from THz-TDS and IRT. The analysis process on raw data from THz-TDS modality includes time-domain and frequency-domain analysis to obtain images by layers owing to the time and spectral characteristics on different materials, while information from different depths on the specimens is collected with the thermal diffusion process on optical excitation thermography. Furthermore, an unsupervised deep residual fusion algorithm is adapted to merge information from two different techniques. The fusion results are reconstructed in a 3D form to show the through-depth exhibition of the materials.

Due to the complex structure of the plant fibre composites, an effective high-resolution imaging technique is still a key research topic in the composite research area. The main contribution of this study is the proposal of a novel imaging technique based on THz-TDS and IRT data fusion. A spatial resolution of 0.5 mm has been achieved in the final output results. In addition, an unsupervised deep residual fusion algorithm introduced here can effectively merge the salient features from different imaging techniques. Furthermore, the 3D reconstruction result offers a better understanding of the characteristics of the composites. The results and discussion present the 3D fusion imaging results with the X-ray CT inspection, which proves that the proposed 3D fusion

imaging technique offers a promising performance for the imaging of different layers in such complex composite structures.

Acknowledgements

This research was supported by the Natural Sciences and Engineering Research Council (NSERC) Canada through Discovery and CREATE 'oN DuTy!' programs as well as Canada Research Chair in Multipolar Infrared Vision (MiViM)

This research was also supported by the Harbin Institute of Technology through the Young Scientist Studio program..

References

[1] De Rosa IM, Santulli C, Sarasini F. Acoustic emission for monitoring the mechanical behaviour of natural fibre composites: A literature review. Compos Part a Appl Sci Manuf 2009;40:1456–69.

[2] Cawley P. Inspection of composites--current status and challenges. Proc 9th ECNDT, Berlin 2006.

[3] Sfarra S, Ibarra-Castanedo C, Santulli C, Paoletti A, Paoletti D, Sarasini F, et al. Falling weight impacted glass and basalt fibre woven composites inspected using non-destructive techniques. Compos Part B Eng 2013;45:601–8.

[4] Gholizadeh S. A review of non-destructive testing methods of composite materials. Procedia Struct Integr 2016;1:50–7.

[5] Duchene P, Chaki S, Ayadi A, Krawczak P. A review of non-destructive techniques used for mechanical damage assessment in polymer composites. J Mater Sci 2018;53:7915–38.

[6] Ali MA, Umer R, Khan KA, Cantwell WJ. Application of X-ray computed tomography for the virtual permeability prediction of fiber reinforcements for liquid composite molding processes: A review. Compos Sci Technol 2019:107828.

[7] Jördens C, Wietzke S, Scheller M, Koch M. Investigation of the water absorption in polyamide and wood plastic composite by terahertz time-domain spectroscopy. Polym Test 2010;29:209–15.

[8] Zhang H, Sfarra S, Osman A, Szielasko K, Stumm C, Genest M, et al. An infrared-induced terahertz imaging modality for foreign object detection in a lightweight honeycomb composite structure. IEEE Trans Ind Informatics 2018;14:5629–36.

[9] Yang R, He Y. Optically and non-optically excited thermography for composites: A review. Infrared Phys Technol 2016;75:26–50.

[10] Ciampa F, Mahmoodi P, Pinto F, Meo M. Recent advances in active infrared thermography for non-destructive testing of aerospace components. Sensors 2018;18:609.

[11] Zhang H, Robitaille F, Grosse CU, Ibarra-Castanedo C, Martins JO, Sfarra S, et al. Optical excitation thermography for twill/plain weaves and stitched fabric dry carbon fibre preform inspection. Compos Part A Appl Sci Manuf 2018;107:282–93.

[12] Zhang H, Verberne P, Meguid SA, Ibarra-Castanedo C, Maldague XP V. Autonomous high resolution inspection of kiss-bonds skins of carbon nanotube reinforced nanocomposites using novel dynamic line-scan thermography approach. Compos Sci Technol 2020;192:108111.

[13] Zhang H, Yu L, Hassler U, Fernandes H, Genest M, Robitaille F, et al. An experimental and analytical study of micro-laser line thermography on micro-sized flaws in stitched carbon fiber reinforced polymer composites. Compos Sci Technol 2016;126:17–26.

[14] Zhang X, He Y, Chady T, Tian G, Gao J, Wang H, et al. CFRP impact damage inspection based on manifold learning using ultrasonic induced thermography. IEEE Trans Ind Informatics 2018;15:2648–59.

[15] He Y, Tian G, Pan M, Chen D. Impact evaluation in carbon fiber reinforced plastic (CFRP) laminates using eddy current pulsed thermography. Compos Struct 2014;109:1–7.

[16] Ibarra-Castanedo C, Maldague XP V. Infrared thermography. Handb. Tech. diagnostics, Springer; 2013, p. 175–220.

[17] Chady T, Lopato P. Testing of glass-fiber reinforced composite materials using terahertz technique. Int J Appl Electromagn Mech 2010;33:1599–605.

[18] Zhang J, Shi C, Ma Y, Han X, Li W, Chang T, et al. Spectroscopic study of terahertz reflection and transmission properties of carbon-fiber-reinforced plastic composites. Opt Eng 2015;54:54106.

[19] Zhang J, Chen J, Wang J, Lang J, Zhang J, Shen Y, et al. Nondestructive evaluation of glass fiber honeycomb sandwich panels using reflective terahertz imaging. J Sandw Struct \& Mater 2019;21:1211–23.

[20] Liu Z, Forsyth DS, Komorowski JP, Hanasaki K, Kirubarajan T. Survey: State of the art in NDE data fusion techniques. IEEE Trans Instrum Meas 2007;56:2435–51.

[21] Wang J, Xu T, Zhang L, Chang T, Zhang J, Yan S, et al. Nondestructive damage evaluation of composites based on terahertz and X-ray image fusion. NDT \& E Int 2022:102616.

[22] Akil HM, De Rosa IM, Santulli C, Sarasini F. Flexural behaviour of pultruded jute/glass and kenaf/glass hybrid composites monitored using acoustic emission. Mater Sci Eng A 2010;527:2942–50.

[23] He K, Zhang X, Ren S, Sun J. Deep residual learning for image recognition. Proc. IEEE Conf. Comput. Vis. pattern Recognit., 2016, p. 770–8.

[24] Li H, Wu X-J. Densefuse: A fusion approach to infrared and visible images. IEEE Trans Image Process 2018;28:2614–23.

[25] Wang Z, Bovik AC, Sheikh HR, Simoncelli EP, others. Image quality assessment: from error visibility to structural similarity. IEEE Trans Image Process 2004;13:600–12.

[26] Lin T-Y, Maire M, Belongie S, Hays J, Perona P, Ramanan D, et al. Microsoft coco: Common objects in context. Eur. Conf. Comput. Vis., 2014, p. 740–55.

[27] Redo-Sanchez A, Heshmat B, Aghasi A, Naqvi S, Zhang M, Romberg J, et al. Terahertz time-gated spectral imaging for content extraction through layered structures. Nat Commun 2016;7:1–7.

Highlights

1) A novel infrared-terahertz fusion non-invasive imaging technique was proposed for 3D inspection of plant fibre-reinforced polymer composites.

2) An unsupervised deep residual fusion algorithm was proposed to merge the information from terahertz time-domain spectroscopy and infrared thermography.

3) The proposed fusion imaging technique achieves high resolution and high contrast imaging on internal layers from complementary depths of different systems.

4) The reconstructed 3D fusion slices with spatial resolution of 0.5 mm were compared with X-ray CT, which proves the capability of the new technique.

Declaration of interests

☒ The authors declare that they have no known competing financial interests or personal relationships that could have appeared to influence the work reported in this paper.

☐The authors declare the following financial interests/personal relationships which may be considered as potential competing interests: